Operation of a superconducting nanowire quantum interference device with mesoscopic leads

David Pekker, Alexey Bezryadin, David S. Hopkins, and Paul M. Goldbart
Department of Physics, University of Illinois at Urbana-Champaign, 1110 West Green Street, Urbana, Illinois 61801-3080, USA
(Received 14 July 2005; published 27 September 2005)

A theory describing the operation of a superconducting nanowire quantum interference device (NQUID) is presented. The device consists of a pair of thin-film superconducting leads connected by a pair of topologically parallel ultranarrow superconducting wires. It exhibits intrinsic electrical resistance, due to thermally activated dissipative fluctuations of the superconducting order parameter. Attention is given to the dependence of this resistance on the strength of an externally applied magnetic field aligned perpendicular to the leads, for lead dimensions such that there is essentially complete and uniform penetration of the leads by the magnetic field. This regime, in which at least one of the lead dimensions—length or width—lies between the superconducting coherence and penetration lengths, is referred to as the *mesoscopic* regime. The magnetic field causes a pronounced oscillation of the device resistance, with a period *not* dominated by the Aharonov-Bohm effect through the area enclosed by the wires and the film edges but, rather, in terms of the geometry of the leads, in contrast to the well-known Little-Parks resistance of thin-walled superconducting cylinders. A detailed theory, encompassing this phenomenology quantitatively, is developed through extensions, to the setting of parallel superconducting wires, of the Ivanchenko-Zil'berman-Ambegaokar-Halperin theory of intrinsic resistive fluctuations in a current-biased Josephson junction and the Langer-Ambegaokar-McCumber-Halperin theory of intrinsic resistive fluctuations in a superconducting wire. In particular, it is demonstrated that via the resistance of the NQUID, the wires act as a probe of spatial variations in the superconducting order parameter along the perimeter of each lead: in essence, a superconducting phase gradiometer.

DOI: 10.1103/PhysRevB.72.104517 PACS number(s): 74.78.Na, 85.25.Dq, 85.65.+h

I. INTRODUCTION

The Little-Parks effect concerns the electrical resistance of a thin cylindrically shaped superconducting film and, specifically, the dependence of this resistance on the magnetic flux threading the cylinder.[1,2] It is found that the resistance is a periodic function of the magnetic field, with period inversely proportional to the cross-sectional area of the cylinder. Similarly, in a dc SQUID, the critical value of the supercurrent is periodic in magnetic field, with period inversely proportional to the area enclosed by the SQUID ring.[2]

In this paper, we consider a mesoscopic analog of a dc SQUID. The analog consists of a device composed of a thin superconducting film patterned into two mesoscopic leads that are connected by a pair of (topologically) parallel, short, weak, superconducting wires. Thus, we refer to the device as an NQUID (superconducting nanowire quantum interference device). The only restriction that we place on the wires of the device is that they be thin enough for the order parameter to be taken as constant over each cross section of a wire, varying only along the wire length. In principle, this condition of one-dimensionality is satisfied if the wire is much thinner than the superconducting coherence length ξ. In practice, it is approximately satisfied provided the wire diameter d is smaller than 4.4ξ.[3] For thicker wires, vortices can exist inside the wires, and such wires may not be assumed to be one-dimensional.

By the term *mesoscopic* we are characterizing phenomena that occur on length scales larger than the superconducting coherence length ξ but smaller than the electromagnetic penetration depth $\lambda_\perp$ associated with magnetic fields applied perpendicular to the superconducting film. We shall call a lead mesoscopic if at least one of its two long dimensions is in the mesoscopic regime; the other dimension may be either mesoscopic or macroscopic. Thus, a weak magnetic field applied perpendicular to a mesoscopic lead will penetrate the lead without appreciable attenuation and without driving the lead from the homogeneous superconducting state to the Abrikosov vortex state. This is similar to the regime of operation of superconducting wire networks; see, e.g., Ref. 4. The nanowires connecting the two leads are taken to be topologically parallel (i.e., parallel in the sense of electrical circuitry): these nanowires and edges of the leads define a closed geometrical contour, which will be referred to as the *Aharonov-Bohm (AB) contour*. In our approach, the nanowires are considered to be links sufficiently weak that any effects of the nanowires on the superconductivity in the leads can be safely ignored.

The theory presented here has been developed to explain experiments conducted on DNA-templated NQUIDs.[5] These experiments measure the electrical resistivity of a pair of superconducting nanowires suspended between long superconducting strips (see Fig. 1). In them, a current source is

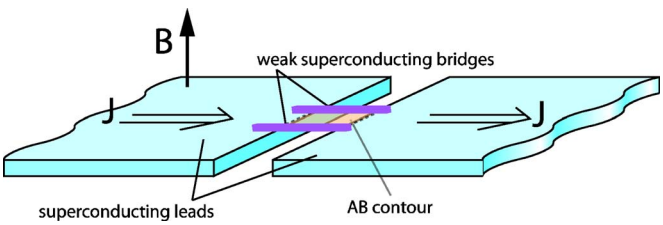

FIG. 1. (Color online) Schematic depiction of the superconducting phase gradiometer. A current J is passed through the bridges in the presence of a perpendicular magnetic field of strength B.

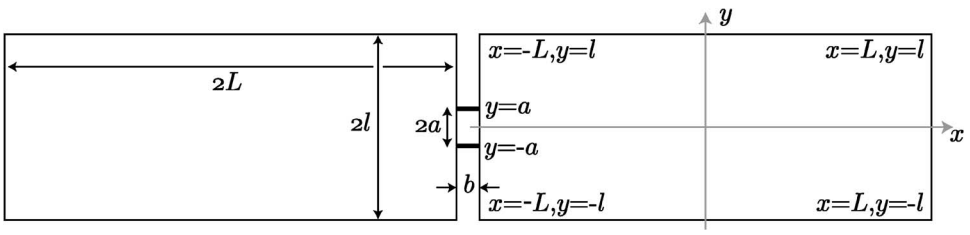

FIG. 2. Geometry of the two-wire device, showing the dimensions. The coordinate system used for the right lead (with the origin in the center of the lead) is also shown. The coordinates of the four corners of the right lead, as well as the coordinates of the points at which the two wires are connected to the right lead, are indicated. As shown, we always assume that the wires are attached near the center of the short edges of the leads.

used to pass dc current from a contact on the far end of the left lead to one on the far end of the right lead. The voltage between the contacts is measured (and the resistance is hence determined) as a function of the magnetic field applied perpendicular to the plane of the strips.

In light of the foregoing remarks, the multiple connectedness of the device suggests that one should anticipate oscillations with magnetic field, e.g., in the device resistance. Oscillations are indeed observed. But they are distinct from the resistance oscillations observed by Little and Parks and from the critical current oscillations observed in SQUID rings. What distinguishes the resistance oscillations reported in Ref. 5 from those found, e.g., by Little and Parks? First, the most notable aspect of these oscillations is the value of their period. In the Little-Parks type of experiment, the period is given by $\Phi_0/2ab$, where $\Phi_0(\equiv hc/2e)$ is the superconducting flux quantum, $2a$ is the bridge separation, and b is the bridge length, i.e., the superconducting flux quantum divided by the area of the AB contour (see Fig. 2). In a high-magnetic-field regime, such periodic behavior is indeed observed experimentally, with the length of the period somewhat shorter but of the same order of magnitude as in the AB effect.[5] However, in a low-magnetic-field regime, the observed period is appreciably smaller (in fact by almost two orders of magnitude for our device geometry). Second, because the resistance is caused by thermal phase fluctuations (i.e., phase slips) in very narrow wires, the oscillations are observable over a wide range of temperatures ($\sim$1 K). Third, the Little-Parks resistance is wholly ascribed to a rigid shift of the $R(T)$ curve with magnetic field, as T_c oscillates. In contrast, in our system we observe a periodic broadening of the transition (instead of the Little-Parks–type rigid shift) with magnetic field. Our theory explains quantitatively this broadening via the modulation of the barrier heights for phase slips of the superconducting order parameter in the nanowires.

In the experiment, the sample is cooled in zero magnetic field, and the field is then slowly increased while the resistance is measured. At a sample-dependent field ($\sim$5 mT), the behavior switches sharply from a low-field to a high-field regime. If the high-field regime is not reached before the magnetic field is swept back, the low-field resistance curve is reproduced. However, once the high-field regime has been reached, the sweeping back of the field reveals phase shifts and hysteresis in the $R(B)$ curve. The experiments[5] mainly address rectangular leads that have one mesoscopic and one macroscopic dimension. Therefore, we shall concentrate on such strip geometries. We shall, however, also discuss how to extend our approach to generic (mesoscopic) lead shapes. We note in passing that efficient numerical methods, such as the boundary element method (BEM),[6] are available for solving the corresponding Laplace problems.

This paper is arranged as follows. In Sec. II, we construct a basic picture for the period of the magnetoresistance oscillations of the two-wire device, which shows how the mesoscopic size of the leads accounts for the anomalously short magnetoresistance period in the low-field regime. In Sec. III, we concentrate on the properties of mesoscopic leads with regard to their response to an applied magnetic field, and in Sec. IV, we extend the Langer-Ambegaokar-McCumber-Halperin (LAMH) model to take into account the interwire coupling through the leads. Analytical expressions are derived for the short- and long-wire limits, while a numerical procedure is described for the general case. The predictions of the model are compared with data from our experiment in Sec. V, and we give some concluding remarks in Sec. VI. Certain technical components are relegated to the Appendix, as is the analysis of example multiwire devices.

II. ORIGIN OF MAGNETORESISTANCE OSCILLATIONS

Before presenting a detailed development of the theory, we give an intuitive argument to account for the anomalously short period of the magnetoresistance in the low-magnetic-field regime, mentioned above.

A. Device geometry

The geometry of the devices studied experimentally is shown in Fig. 2. Five devices were successfully fabricated and measured. The dimensions of these devices are listed in Table I, along with the short magnetoresistance oscillation period. The perpendicular penetration depth $\lambda_\perp$ for the films used to make the leads is roughly 70 μm, and coherence length ξ is roughly 5 nm.

B. Parametric control of the state of the wires by the leads

The essential ingredients in our model are (i) leads, in which the applied magnetic field induces supercurrents and hence gradients in the phase of the order parameter, and (ii) the two wires, whose behavior is controlled parametrically by the leads through the boundary conditions imposed by the

TABLE I. Comparison between measured and theoretical magnetoresistance periods. The geometries of the samples were obtained via scanning electron microscopy and used to compute the periods theoretically; see the text for additional details.

Sample	b (nm)	$2a$ (nm)	$2l$ (nm)	Theoretical period (μT)	Measured period (μT)	Error
205-4	121	266	11267	929.21	947	1.9%
219-4	137	594	12062	388.73	456.6	12.8%
930-1	141	2453	14480	78.41	77.5	−1.2%
930-1 (shaved)	141	2453	8930	127.14	128.3	0.9%
205-2	134	4046	14521	47.41	48.9	3.0%

leads on the phase of the order parameters in the wires. For now, we assume that the wires have sufficiently small cross sections that the currents through them do not feed back on the order parameter in the leads. (In Sec. III D, we shall discuss when this assumption may be relaxed without altering the oscillation period.) The dissipation results from thermally activated phase slips, which cause the superconducting order parameter to explore a discrete family of local minima of the free energy. (We assume that the barriers separating these minima are sufficiently high to make them well-defined states.) These minima (and the saddle-point configurations connecting them) may be indexed by the net (i.e., forward minus reverse) number of phase slips that have occurred in each wire (n_1 and n_2, relative to some reference state). More usefully, they can be indexed by $n_s=\min(n_1,n_2)$ (i.e., the net number of phase slips that have occurred in both wires) and $n_v=n_1-n_2$ (i.e., the number of vortices enclosed by the AB contour, which is formed by the wires and the edges of the leads). We note that two configurations with identical n_v but distinct n_s and n_s' have identical order parameters, but differ in energy by

$$\int IVdt = \frac{\hbar}{2e}\int I\dot{\Theta}dt = \frac{h}{2e}I(n_s' - n_s), \tag{1}$$

due to the work done by the current source supplying the current I, in which V is the interlead voltage, Θ is the interlead phase difference as measured between the two points halfway between the wires, and the Josephson relation $\dot{\Theta}=2eV/\hbar$ has been invoked. In our model, we assume that the leads are completely rigid. Therefore, the rate of phase change, and thus the voltage, is identical at all points inside one lead. For sufficiently short wires, n_v has a unique value, as there are no stable states with any other number of vortices.

Due to the screening currents in the left lead, induced by the applied magnetic field B (and independent of the wires), there is a field-dependent phase $\delta_{2\leftarrow 1,L}(B)=\int_1^2 d\vec{r}\cdot\vec{\nabla}\varphi(B)$ (computed below) accumulated in passing from the point at which wire 1 (the top wire) contacts the left (L) lead to the point at which wire 2 (the bottom wire) contacts the left lead (see Fig. 3). Similarly, the field creates a phase accumulation $\delta_{2\leftarrow 1,R}(B)$ between the contact points in the right (R) lead. As the leads are taken to be geometrically identical, the phase accumulations in them differ in sign only: $\delta_{2\leftarrow 1,L}(B)=-\delta_{2\leftarrow 1,R}(B)$. We introduce $\delta(B)=\delta_{2\leftarrow 1,L}(B)$. In determining the local free-energy minima of the wires, we solve the Ginzburg-Landau equation for the wires for each vortex number n_v, imposing the single-valuedness condition on the order parameter,

$$\theta_{1,L\leftarrow R} - \theta_{2,L\leftarrow R} + 2\delta(B) = 2\pi n_v. \tag{2}$$

This condition will be referred to as the *phase constraint*. Here, $\theta_{1,L\leftarrow R}=\int_R^L d\vec{r}\cdot\vec{\nabla}\varphi(B)$ is the phase accumulated along wire 1 in passing from the right to the left lead; $\theta_{2,L\leftarrow R}$ is similarly defined for wire 2.

Absent any constraints, the lowest-energy configuration of the nanowires is the one with no current through the wires. Here, we adopt the gauge in which $\boldsymbol{A}=By\mathbf{e}_x$ for the electromagnetic vector potential, where the coordinates are as shown in Fig. 2. The Ginzburg-Landau expression for the current density in a superconductor is

$$\boldsymbol{J} \propto \left(\boldsymbol{\nabla}\varphi(\boldsymbol{r}) - \frac{2e}{\hbar}\boldsymbol{A}(\boldsymbol{r})\right). \tag{3}$$

For our choice of gauge, the vector potential is always parallel to the nanowires, and therefore the lowest-energy state of the nanowires corresponds to a phase accumulation given by the flux through the AB contour, $\theta_{1,L\leftarrow R}=-\theta_{2,L\leftarrow R}=2\pi Bab/\Phi_0$. As we shall show shortly, for our device geometry (i.e., when the wires are sufficiently short, i.e., $b\ll l$), this phase accumulation may be safely ignored, compared to the phase accumulation $\delta(B)$ associated with screening currents induced in the leads. As the nanowires are assumed to be weak compared to the leads, to satisfy the phase con-

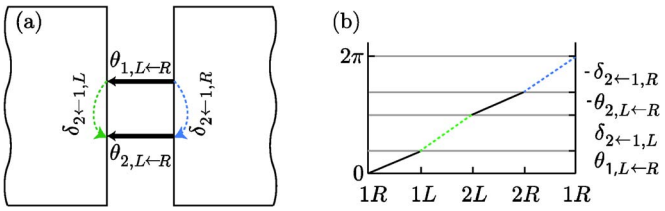

FIG. 3. (Color online) (a) Close-up of the two nanowires and the leads. The top (bottom) thick arrow represents the integration contour for determining the phase accumulation $\theta_{1,L\leftarrow R}(\theta_{2,L\leftarrow R})$ in the first (second) wire. The dotted arrow in the left (right) lead indicates a possible choice of integration contour for determining the phase accumulation $\delta_{2\leftarrow 1,L}(\delta_{2\leftarrow 1,R})$. These contours may be deformed without affecting the values of the various phase accumulations, as long as no vortices are crossed. (b) Sketch of the corresponding superconducting phase at different points along the AB contour when one vortex is located inside the contour.

straint (2), the phase accumulations in the nanowires will typically deviate from their optimal value, generating a circulating current around the AB contour. As a consequence of LAMH theory, this circulating current results in a decrease of the barrier heights for phase slips, and hence an increase in resistance. The period of the observed oscillations is derived from the fact that whenever the magnetic field satisfies the relation

$$2\pi m = 2\pi \frac{2abB}{\Phi_0} + 2\delta(B) \tag{4}$$

[where m is an integer and the factor of 2 accompanying $\delta(B)$ reflects the presence of two leads], there is no circulating current in the lowest-energy state, resulting in minimal resistance. Furthermore, the family of free-energy minima of the two-wire system (all of which, in thermal equilibrium, are statistically populated according to their energies) is identical to the $B=0$ case. The mapping between configurations at zero and nonzero B fields is established by a shift of the index $n_v \rightarrow n_v - m$. Therefore, as the sets of physical states of the wires are identical whenever the periodicity condition (4) is satisfied, at such values of B the resistance returns to its $B=0$ value.

C. Simple estimate of the oscillation period

In this subsection, we will give a "back of the envelope" estimate for the phase gain $\delta(B)$ in a lead by considering the current and phase profiles in one such lead. According to the Ginzburg-Landau theory, in a mesoscopic superconductor, subjected to a weak magnetic field, the current density is given by Eq. (3). Now consider an isolated strip-shaped lead used in the device. Far from either of the short edges of this lead, $\boldsymbol{A}=By\boldsymbol{e}_x$ is a London gauge,[7] i.e., along all surfaces of the superconductor $\boldsymbol{A}$ is parallel to them; $\boldsymbol{A}\rightarrow\boldsymbol{0}$ in the center of the superconductor; and $\boldsymbol{\nabla}\cdot\boldsymbol{A}=\boldsymbol{0}$. In this special case, the London relation[20] states that the supercurrent density is proportional to the vector potential in the London gauge. Using this relation, we find that the supercurrent density is $\boldsymbol{J}\propto -(2e/\hbar)\boldsymbol{A}=-(2e/\hbar)By\boldsymbol{e}_x$, i.e., there is a supercurrent density of magnitude $\propto(2e/\hbar)Bl$ flowing to the left at the top (long) edge of the strip and to the right at the bottom (long) edge. At the two short ends of the strip, the two supercurrents must be connected, so there is a supercurrent density of magnitude $\sim(2e/\hbar)Bl$ flowing down the left (short) edge of the strip and up the right (short) edge (see Fig. 4). Near the short ends of the strips, our choice of gauge no longer satisfies the criteria for being a London gauge, and therefore $\boldsymbol{\nabla}\phi$ may be nonzero. As in our choice of gauge $\boldsymbol{A}$ points in the $\boldsymbol{e}_x$ direction, the supercurrent on the ends of the strip along $\boldsymbol{e}_y$ must come from the $\nabla_y\phi$ term. Near the center of the short edge $\nabla_y\phi=-2\pi c_1 l/\Phi_0 B$. The phase difference between the points $(-L,-a)$ and $(-L,a)$ is therefore given by

$$\delta(B) = \int_{-a}^{a} \nabla_y \phi dy = -\frac{2\pi c_1}{\Phi_0} B 2al, \tag{5}$$

where we have substituted $2\pi/\Phi_0$ for $2e/\hbar$ and $c_1(a/l)$ is a function of order unity, which accounts for how the current flows around the corners. As we shall show, c_1 depends only weakly on a/l, and is constant in the limit $a \ll l$.

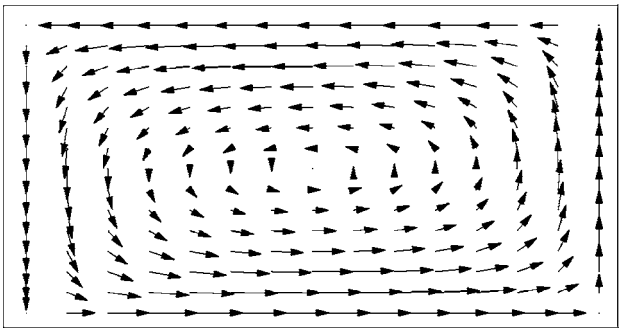

FIG. 4. Current profile in a long superconducting strip, calculated for a finite-length strip by summing the series for $\boldsymbol{\nabla}\phi - (2\pi/\Phi_0)\boldsymbol{A}$ [from Eq. (15)] numerically. Note that there is no vortex in the center of the lead.

Finally, we obtain the magnetoresistance period by substituting Eq. (5) into Eq. (4),

$$\Delta B = \left[\left(\frac{\Phi_0}{c_1 4al} \right)^{-1} + \left(\frac{\Phi_0}{2ab} \right)^{-1} \right]^{-1}. \tag{6}$$

Thus, we see that for certain geometries the period is largely determined not by the flux threading through the geometric area $2ab$ but by the response of the leads and the corresponding effective area $4al$, provided the nanowires are sufficiently short (i.e., $b \ll l$), justifying our assumption of ignoring the phase gradient induced in the nanowires by the magnetic field.

In fact, we can also make a prediction for the periodicity of the magnetoresistance at high magnetic fields, i.e., when vortices have penetrated the leads (see Sec. III A). To do this, we should replace l in Eq. (6) by the characteristic intervortex spacing r. Note that if r is comparable to b, we can no longer ignore the flux through the AB contour. Furthermore, if $r \ll b$, then the flux through the AB contour determines periodicity and one recovers the usual Aharonov-Bohm type of phenomenology.

III. MESOSCALE SUPERCONDUCTING LEADS

In this section and the following one, we shall develop a detailed model of the leads and nanowires that constitute the mesoscopic device.

A. Vortex-free and vorticial regimes

Two distinct regimes of magnetic field are expected, depending on whether there are trapped (i.e., locally stable) vortices inside the leads. As described by Likharev,[8] a vortex inside a superconducting strip-shaped lead is subject to two forces. First, due to the currents induced by the magnetic field, there is a Magnus force pushing it toward the middle of the strip. Second, there is a force due to image vortices (which are required to enforce the boundary condition that no current flows out of the strip and into the vacuum) pulling the vortex toward the edge. When the two forces balance at

the edge of the strip, there is no energy barrier preventing vortex penetration and vortices enter. Likharev has estimated the corresponding critical magnetic field to be

$$H_s \approx \frac{\Phi_0}{\pi d}\frac{1}{\xi a(1)}, \tag{7}$$

where d ($\equiv 2l$) is the width of the strip and $a(1)\sim 1$ for strips that are much narrower than the penetration depth (i.e., for $d \ll \lambda$).

Likharev has also shown that, once inside a strip, vortices remain stable inside it down to a much lower magnetic field H_{c1}, given by

$$H_{c1} = \frac{\Phi_0}{\pi d}\frac{2}{d}\ln\left(\frac{d}{4\xi}\right). \tag{8}$$

At fields above H_{c1}, the potential energy of a vortex inside the strip is lower than for one outside (i.e., for a virtual vortex[9]). Therefore, for magnetic fields in the range $H_{c1} < H < H_s$, vortices would remain trapped inside the strip, but only if at some previous time the field were larger than H_s. This indicates that hysteresis with respect to magnetic-field variations should be observed, once H exceeds H_s and vortices become trapped in the leads.

In real samples, in addition to the effects analyzed by Likharev, there are also likely to be locations (e.g., structural defects) that can pin vortices, even for fields smaller than H_{c1}, so the reproducibility of the resistance versus field curve is not generally expected once H_s has been surpassed.

As the magnetic field at which vortices first enter the leads is sensitive to the properties of their edges, we expect only rough agreement with Likharev's theory. For sample 219-4, using Likharev's formula, we estimate $H_s = 11$ mT (with $\xi = 5$ nm). The change in regime from fast to slow oscillations is found to occur at 3.1 mT for that sample.[5] It is possible to determine the critical magnetic fields H_s and H_{c1} by the direct imaging of vortices. Although we do not know of such a direct measurement of H_s, H_{c1} was determined by field cooling niobium strips, and found to agree in magnitude with Likharev's estimate.[10]

B. Phase variation along the edge of the lead

In the previous section it was shown that the periodicity of the magnetoresistance is due to the phase accumulations associated with the currents along the edges of the leads between the nanowires. Thus, we should make a precise calculation of the dependence of these currents on the magnetic field, and this we now do.

1. Ginzburg-Landau theory

To compute $\delta(B)$, we start with the Ginzburg-Landau equation for a thin film as our description of the mesoscopic superconducting leads,

$$\alpha\psi + \beta|\psi|^2\psi + \frac{1}{2m^*}\left(\frac{\hbar}{i}\nabla - \frac{e^*}{c}\boldsymbol{A}\right)^2\psi = 0. \tag{9}$$

Here, ψ is the Ginzburg-Landau order parameter, $e^*(=2e)$ is the charge of a Cooper pair and m^* is its mass, and α and β may be expressed in terms of the coherence length ξ and critical field H_c via $\alpha = -\hbar^2/2m^*\xi^2$ and $\beta = 4\pi\alpha^2/H_c^2$.

The assumptions that the magnetic field is sufficiently weak and that the lead is a narrow strip (compared with the magnetic penetration depth) allow us to take the *amplitude* of the order parameter in the leads to have the value appropriate to an infinite thin film in the absence of the field. By expressing the order parameter in terms of the (constant) amplitude ψ_0 and the (position-dependent) phase $\phi(\boldsymbol{r})$, i.e.,

$$\psi(\boldsymbol{r}) = \psi_0 e^{i\phi(\boldsymbol{r})}, \tag{10}$$

the Ginzburg-Landau formula for the current density,

$$\boldsymbol{J} = \frac{e^*\hbar}{2m^* i}(\psi^*\nabla\psi - \psi\nabla\psi^*) - \frac{e^{*2}}{m^* c}\psi^*\psi\boldsymbol{A}(\boldsymbol{r}), \tag{11}$$

becomes

$$\boldsymbol{J} = \frac{e^*}{m^*}\psi_0^2\left(\hbar\nabla\phi(\boldsymbol{r}) - \frac{e^*}{c}\boldsymbol{A}(\boldsymbol{r})\right), \tag{12}$$

and (after dividing by $e^{i\phi(\boldsymbol{r})}$) the real and imaginary parts of the Ginzburg-Landau equation become

$$0 = \left[\alpha\psi_0 + \beta\psi_0^3 + \frac{1}{2m^*}\psi_0\left|\hbar\nabla\phi(\boldsymbol{r}) - \frac{e^*}{c}\boldsymbol{A}(\boldsymbol{r})\right|^2\right], \tag{13a}$$

$$0 = \frac{\hbar^2}{2m^* i}\psi_0\left(\nabla^2\phi(\boldsymbol{r}) - \frac{e^*}{\hbar c}\nabla\cdot\boldsymbol{A}(\boldsymbol{r})\right). \tag{13b}$$

As long as any spatial inhomogeneity in the gauge-covariant derivative of the phase is weak on the length scale of the coherence length [i.e., $\xi|\nabla\phi(\boldsymbol{r}) - (e^*/\hbar c)\boldsymbol{A}(\boldsymbol{r})| \ll 1$], the third term in Eq. (13a) is much smaller than the first two and may be ignored, fixing the amplitude of the order parameter at its field-free infinite thin-film value, viz., $\bar{\psi}_0 \equiv \sqrt{-\alpha/\beta}$. To compute $\phi(\boldsymbol{r})$, we need to solve the imaginary part of the Ginzburg-Landau equation.

2. Formulation as a Laplace problem

We continue to work in the approximation that the amplitude of the order parameter is fixed at $\bar{\psi}_0$. Starting from Eq. (13b), we see that for our choice of gauge, $\boldsymbol{A} = By\boldsymbol{e}_x$, the phase of the order parameter satisfies the Laplace equation, $\nabla^2\phi = 0$. We also enforce the boundary condition that no current flows out of the superconductor on boundary surface Σ, whose normal is $\mathbf{n}$,

$$\boldsymbol{n}\cdot\boldsymbol{j}|_\Sigma = 0, \tag{14a}$$

$$\boldsymbol{j} \propto \left(\nabla\phi - \frac{2\pi}{\Phi_0}\boldsymbol{A}\right). \tag{14b}$$

3. Solving the Laplace problem for the strip geometry

To solidify the intuition gained via the physical arguments given in Sec. II, we now determine the phase profile for an

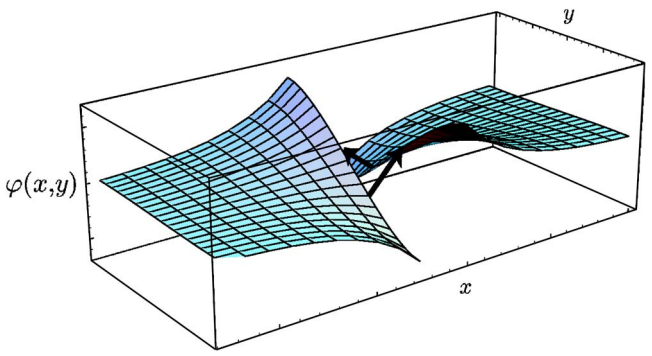

FIG. 5. (Color online) Phase profile in the leads in the vicinity of the trench, generated by numerically summing the series for ϕ for a finite-length strip. Arrows indicate phases connected by nanowires.

isolated superconducting strip in a magnetic field. This will allow us to determine the constant c_1 in Eq. (6), and hence obtain a precise formula for the magnetoresistance period. To this end, we solve Laplace's equation for ϕ subject to the boundary conditions (14). We specialize to the case of a rectangular strip.[21]

In terms of the coordinates defined in Fig. 2, we expand $\phi(x,y)$ as the superposition

$$\phi(x,y) = \Theta_{\mathrm{L/R}} + \sum_k (A_k e^{-kx} + B_k e^{kx}) \sin(ky), \qquad (15)$$

which automatically satisfies Laplace's equation, although the boundary conditions remain to be satisfied. $\Theta_{L(R)}$ is the phase at the the point in the left (right) lead located halfway between the wires. In other words, $\Theta_L = \phi(-L-b,0)$ and $\Theta_R = \phi(-L,0)$ in the coordinate system indicated in Fig. 2. $\Theta_{L/R}$ are not determined by the Laplace equation and boundary conditions, but will be determined later by the state of the nanowires.

We continue working in the gauge $\boldsymbol{A} = By\boldsymbol{e}_x$. The boundary conditions across the edges at $y = \pm l$ (i.e., the long edges) are $\partial_y \phi(x, y = \pm l) = 0$. These conditions are satisfied by enforcing $k_n = \pi(n + \frac{1}{2})/l$, where $n = 0, 1, 2, \ldots$. The boundary conditions across the edges at $x = \pm L$ (i.e., the short edges) are $\partial_x \phi(x = \pm L, y) = hy$ (where $h \equiv 2\pi B/\Phi_0$). This leads to the coefficients in Eq. (15) taking the values

$$B_k = -A_k = \frac{h}{k_n^3 l} \frac{(-1)^n}{\cosh(k_n L)} \quad (n = 0, 1, \ldots), \qquad (16)$$

and hence to the solution

$$\phi(x,y) = \sum_{n=0}^{\infty} \frac{(-1)^n 2h}{k_n^3 l \cosh(k_n L)} \sin(k_n y) \sinh(k_n x). \qquad (17)$$

Figure 5 shows the phase profiles in the leads, in the region close to the trench that separates the leads.

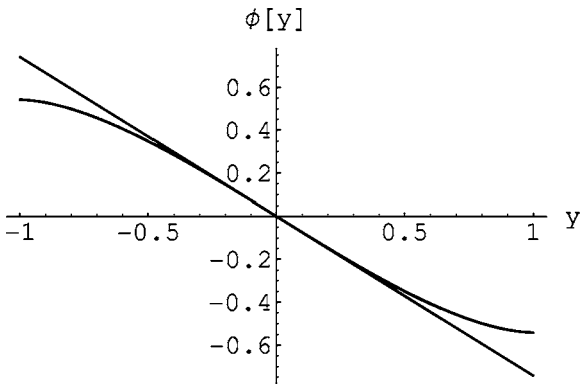

FIG. 6. Phase profile on the $x = -L$ (i.e., short) edge of the strip. Numerical summation [Eq. (18) with 100 terms] for $L = 2$ and $L = \infty$ ($l = 1$) as well as the linear form from Eq. (20). Note that the linear fit is good near the origin (e.g., for $a \lesssim 0.25l$), and the curves for $L = 2$ and $L = \infty$ coincide.

C. Period of magnetoresistance for leads having a rectangular strip geometry

Using the result for the phase that we have just established, we see that the phase profile on the short edge of the strip at $x = -L$ is given by

$$\phi(-L,y) = -\frac{2hl^2}{\pi^2} \sum_{n=0}^{\infty} \frac{(-1)^n}{\left(n + \frac{1}{2}\right)^3} \sin \frac{\pi\left(n + \frac{1}{2}\right) y}{l}, \qquad (18)$$

where we have taken the limit $L \to \infty$. We would like to evaluate this sum at the points $(x,y) = (-L, \pm a)$. This can be done numerically. For nanowires that are close to each other (i.e., for $a \ll l$), an approximate value can be found analytically by expanding in a power series in a around $y = 0$,

$$\phi(-L,a) = \phi(-L,0) + a \left.\frac{\partial}{\partial y}\phi(-L,y)\right|_{y=0} + \frac{a^2}{2} \left.\frac{\partial^2}{\partial y^2}\phi(-L,y)\right|_{y=0} + O(a^3). \qquad (19)$$

The first and third terms are evidently zero, as ϕ is an odd function of y. The second term can be evaluated by changing the order of summation and differentiation. (Higher-order terms are harder to evaluate, as the changing of the order of summation and differentiation does not work for them.) Thus, to leading order in a we have

$$\phi(-L,a) \approx -\frac{8G}{\pi^2} hla, \qquad (20)$$

where $G \equiv \Sigma_{n=0}^{\infty}[(-1)^n/(2n+1)^2] \approx 0.916$ is the Catalan number (see Ref. 11). This linear approximation is plotted, together with the actual phase profile obtained by the numerical evaluation of Eq. (18), in Fig. 6. Hence, the value of c_1 in Eq. (5) becomes $c_1 = 8G/\pi^2 \approx 0.74$, and Eq. (6) becomes

$$B = \frac{\Phi_0}{2\pi} h = \frac{\pi^2}{8G} \frac{\Phi_0}{4al}. \tag{21}$$

To obtain this result, we used the relation $\delta(B)/2 = \phi(-L, a)$.

D. Bridge-lead coupling

In order to simplify our analysis, we have assumed that the nanowires do not exert any influence on the order parameter in the leads. We examine the justification for this assumption in the setting of the experiment that we are attempting to describe.[5]

The assumption will be valid if the bending of the phase of the order parameter, in order to accommodate any circulating current around the AB contour, occurs largely in the nanowires. As the phase of the order parameter in the leads satisfies the Laplace equation, which is linear, we can superpose the circulating-current solution with the previously obtained magnetic-field-induced solution. The boundary conditions on the right lead for the circulating-current solution are $\boldsymbol{n} \cdot \boldsymbol{\nabla} \phi = 0$ everywhere, except at the two points where the nanowires are attached to the lead [i.e., at $(x, y) = (L, \pm a)$]. Treating the nanowires as point current sources, the boundary condition on the short edge of the right lead is $\partial_x \phi = I(\Phi_0 / H_c^2 s \xi)[\delta(y+a) - \delta(y-a)]$, where I is the current circulating in the loop, and H_c, s, ξ are the film critical field, thickness, and coherence length. By using the same expansion as before, Eq. (15), we obtain the coefficients of the Fourier series in the long strip limit,

$$A_k = I(\Phi_0 / H_c^2 s \xi) \frac{2 \sin(ka)}{kl \exp(kl)}. \tag{22}$$

Having the coefficients of the Fourier series, we can find the phase difference in the right lead between the two points at which the nanowires connect to the right lead, induced in this lead by the current circulating in the loop,

$$\delta_{cc} = 2I(\Phi_0 / H_c^2 s \xi) \sum_{n=0}^{k=1/w} \frac{\sin^2(ka)}{kl} \sim \ln(2l/\pi w). \tag{23}$$

Here, we have introduced a large wave-vector k cutoff at the inverse of the width w of the wire. On the other hand, the current flowing through the wire is

$$\frac{\xi H_{c2}}{\Phi_0} w s \frac{\Delta\theta}{b}, \tag{24}$$

where ξ, H_c, and s are the wire coherence length, critical field, and height (recall that b is the wire length). To support a circulating current that corresponds to a phase accumulation of $\Delta\theta$ along one of the wires, the phase difference between the two nanowires in the lead must be on the order of

$$\delta_{cc} = \Delta\theta \frac{w}{b} \frac{(H_c^2 s \xi)_{\text{wire}}}{(H_c^2 \xi)_{\text{film}}} \ln\left(\frac{2l}{\pi w}\right). \tag{25}$$

For our experiments,[5] we estimate that the ratio of δ_{cc} to $\Delta\theta$ is always less than 20%, validating the assumption of weak coupling.

E. Strong nanowires

We remark that the assumption of weak nanowires *is not obligatory* for the computation of the magnetoresistance *period*. Dropping this assumption would leave the period of the magnetoresistance oscillations unchanged.

To see this, consider ϕ_{11}, i.e., the phase profile in the leads that corresponds to the lowest energy solution of the Ginzburg-Landau equation at field corresponding to the first resistance minimum [i.e., at B being the first nonzero solution of Eq. (4)]. For this case, and for short wires, the phase gain along the wires is negligible, whereas the phase gain in the leads is 2π, even for wires with large critical current. Excited states, with vortices threading the AB contour, can be constructed by the linear superposition of ϕ_{11} with ϕ_{0n_v}, where ϕ_{0n_v} is the phase profile with n_v vortices at no applied magnetic field.

This construction requires that the nanowires are narrow, but works independently of whether nanowires are strong or weak, in the limit that $H \ll H_c$. The energy of the lowest-energy state always reaches its minimum when the applied magnetic field is such that there is no phase gain (i.e., no current) in the nanowires. By the above construction, it is clear that the resistance of the device at this field is the same as at zero field, and therefore the minimum possible.

Therefore, our calculation of the period is valid, independent of whether the nanowires are weak or strong. However, the assumption of weak nanowires is necessary for the computation of magnetoresistance amplitude, which we present in the following section.

IV. PARALLEL SUPERCONDUCTING NANOWIRES AND INTRINSIC RESISTANCE

In this section, we consider the intrinsic resistance of the device. We assume that this resistance is due to thermally activated phase slips (TAPS) of the order parameter, and that these occur within the nanowires. Equivalently, these processes may be thought of as thermally activated vortex flow across the nanowires. Specifically, we shall derive analytical results for the asymptotic cases of nanowires that are either short or long, compared to coherence length, i.e., Josephson junctions[12,13] or Langer-Ambegaokar-McCumber-Halperin (LAMH) wires;[14,15] see also Ref. 16. We have not been able to find a closed-form expression for the intrinsic resistance in the intermediate-length regime, so we shall consider that case numerically.

There are two (limiting) kinds of experiments that may be performed: fixed total current and fixed voltage. In the first kind, a specified current is driven through the device and the time-averaged voltage is measured. Here, this voltage is proportional to the net number of phase slips (in the forward direction) per unit time, which depends on the height of the free-energy barriers for phase slips. Why do we expect minima in the resistance at magnetic fields corresponding to $2\delta = 2m\pi$ and maxima at $2\delta = (2m+1)\pi$ for m integral, at least at vanishingly small total current through both wires? For $2\delta = 2m\pi$, the nanowires are unfrustrated, in the sense that there is no current through either wire in the lowest local

minimum of the free energy. On the other hand, for $2\delta = (2m+1)\pi$ the nanowires are maximally frustrated: there is a nonzero circulating current around the AB contour. Quite generally, the heights of the free-energy barriers protecting locally stable states decrease with increasing current through a wire, and thus the frustrated situation is more susceptible to dissipative fluctuations, and hence shows higher resistance. Note, however, that due to the interbridge coupling caused by the phase constraint, the resistance of the full device is more subtle than the mere addition of the resistances of two independent, parallel nanowires, both carrying the requisite circulating current.

In the second kind of experiment, a fixed voltage is applied across the device and the total current is measured. In this situation, the interlead voltage is fixed, and therefore the phase drop along each wire is a fixed function of time. Hence, there is no interbridge coupling in the fixed voltage regime. Therefore, the resistance of the device would not exhibit a magnetic-field dependence. If the voltage is fixed far away from the wires, but not in the immediate vicinity of the wires, so that the phase drop along each wire is not rigidly fixed, then some of the magnetic-field dependence of the resistance would be restored. In our experiments on two-wire devices, we believe that the situation lies closer to the fixed current limit than to the fixed voltage limit, and therefore we shall restrict our attention to the former limit.

In the fixed current regime, the relevant independent thermodynamic variable for the device is the total current through the pair of wires, i.e., $I \equiv I_1 + I_2$. Therefore, the appropriate free energy to use, in obtaining the barrier heights for phase slips, is the Gibbs free energy $G(I)$, as discussed by McCumber,[17] rather than the Helmholtz free energy $F(\Theta)$.[22] In the Helmholtz free energy, the independent variable can be taken to be $\Theta \equiv \Theta_L - \Theta_R$, i.e., the phase difference across the center of the "trench," defined modulo 2π. $G(I)$ is obtained from $F(\Theta)$ via the appropriate Legendre transformation,

$$G(I) = F(\Theta) - \frac{\hbar}{2e} I\Theta, \tag{26}$$

where the second term represents the work done on the system by the external current source. $F(\Theta)$ is the sum of the Helmholtz free energies for the individual nanowires,

$$F(\Theta) = F_1(\theta_1) + F_2(\theta_2), \tag{27}$$

where $F_{1\ (2)}(\theta_{1\ (2)})$ is the Ginzburg-Landau free energy for first (second) wire and a simplified notation has been used, $\theta_1 \equiv \theta_{1,L\leftarrow R}$ and $\theta_2 \equiv \theta_{2,L\leftarrow R}$. θ_1 and θ_2 are related to each other and to Θ through the phase constraint Eq. (2).

A. Short nanowires: Josephson junction limit

If the nanowires are sufficiently short, they may be treated as Josephson junctions. Unlike the case of long nanowires, described in the following subsection, in this Josephson regime there is no metastability, i.e., the free energy of each junction is a single-valued function of the phase difference, modulo 2π, across it. The phase constraint then implies that there is a rigid difference between the phases across the two junctions. As a consequence, n_v can be set to zero. The Gibbs free energy in such a configuration is then

$$G(I) = -\frac{\hbar}{2e}[I_{c1}\cos(\theta_1) + I_{c2}\cos(\theta_2) + I\Theta], \tag{28}$$

where I_{c1} and I_{c2} are the critical currents for the junctions. In thermodynamic equilibrium, the Gibbs free energy must be minimized, so the dependent variable Θ must be chosen such that $\partial G(I)/\partial\Theta = 0$.

Using $\theta_1 = \Theta + \delta$ and $\theta_2 = \Theta - \delta$, $G(I)$ may be rewritten in the form

$$\tilde{G}(I) = -\frac{\hbar}{2e}[\sqrt{(I_{c1}+I_{c2})^2\cos^2\delta + (I_{c1}-I_{c2})^2\sin^2\delta}\cos(\vartheta) + I\vartheta_1], \tag{29}$$

where we have shifted the free energy by an additive constant

$$\left(\frac{\hbar}{2e}\right) I \tan^{-1}\left[\left(\frac{I_{c1}-I_{c2}}{I_{c2}+I_{c1}}\right)\tan\delta\right]$$

and

$$\vartheta \equiv \Theta + \tan^{-1}\left[\left(\frac{I_{c1}-I_{c2}}{I_{c2}+I_{c1}}\right)\tan\delta\right].$$

In this model, the option for having $I_{c1} \neq I_{c2}$ is kept open. Equation (29) shows that, up to an additive constant, the free energy of the two-junction device is identical to that of an effective single-junction device with an effective I_c, which is given by

$$I_c = \sqrt{(I_{c1}+I_{c2})^2\cos^2\delta + (I_{c1}-I_{c2})^2\sin^2\delta}. \tag{30}$$

Thus, we may determine the resistance of the two-junction device by applying the well-known results for a single junction, established by Ivanchenko and Zil'berman[12] and by Ambegaokar and Halperin,[13]

$$R = R_n \frac{2(1-x^2)^{1/2}}{x} \exp[-\gamma(\sqrt{1-x^2} + x\sin^{-1}x)]\sinh(\pi\gamma x/2), \tag{31a}$$

$$x \equiv I/I_c, \quad \gamma \equiv \hbar I_c/ek_BT, \tag{31b}$$

where R_n is the normal-state resistance of the two-junction device. This formula for R holds when the free-energy barrier is much larger than k_BT, so that the barriers for phase slips are high. References 12 and 13 provide details on how to calculate the resistance in the general case of an overdamped junction, which includes that of shallow barriers. Figure 7 shows the fits to the resistance, computed using Eqs. (30) and (31), as a function of temperature, magnetic field, and total current for sample 219-4. Observe that both the field and the temperature dependence are in good agreement with experimental data. In Sec. V B 2, we make more precise contact between theory and experiment, and explain how the data have been fitted. We also note that, as it should, our Josephson junction model exactly coincides with our ex-

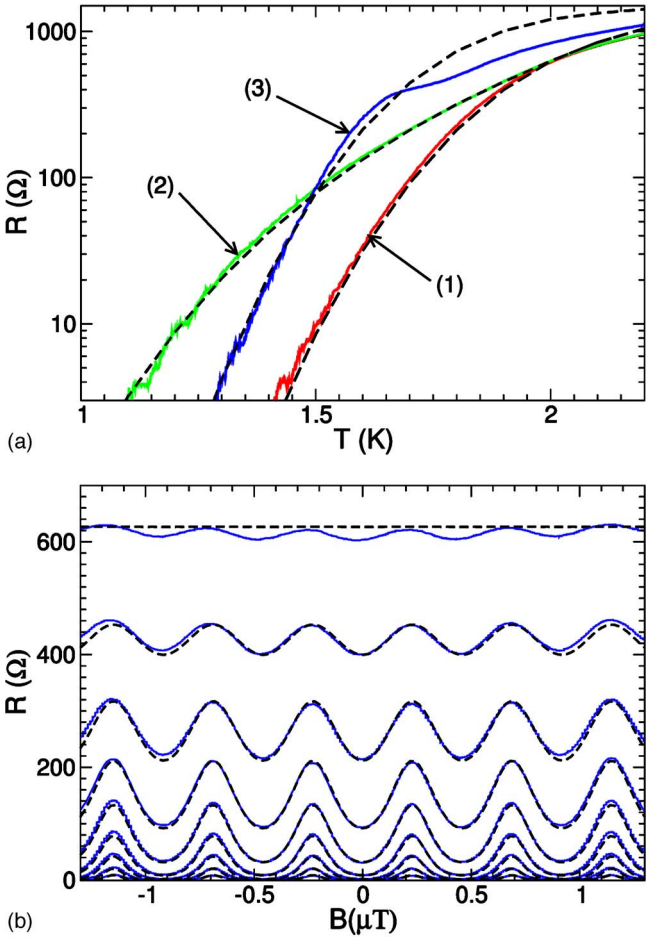

FIG. 7. (Color online) Sample 219-4: Experimental data (solid lines) and theoretical fits using the Josephson junction model (dashed lines). (a) Resistance vs temperature curves. (1) Zero magnetic field and low total current. (2) Magnetic field set to maximize the resistance and low total current. (3) Zero magnetic field and 70 nA total current. (b) Resistance as a function of magnetic field at various temperatures from 1.2 to 2.0 K in 0.1 K increments. The fitting parameters used were $J_{c1}=639$ nA, $J_{c2}=330$ nA, $T_{c1}=2.98$ K, and $T_{c2}=2.00$ K, with corresponding coherence lengths $\xi_1(0)=23$ nm and $\xi_2(0)=30$ nm. Only one set of fitting parameters [derived from curves (1) and (2)] was used to produce all the theoretical curves.

tension of the LAMH model in the limit of very short wires and for temperatures for which the barrier-crossing approximation is valid.

B. Longer nanowires: LAMH regime

In this section, we describe an extension of the LAMH model of resistive fluctuations in a single narrow wire,[14,15] which we shall use to make a quantitative estimate of the voltage across the two-wire device at a fixed total current. In this regime, the nanowires are sufficiently long that they behave as LAMH wires. We shall only dwell on two-wire systems, but we note in passing that the model can straightforwardly be extended to more complicated sets of lead interconnections, including periodic, gratinglike arrays (see Appendix A).

As the sample is not simply connected, i.e., there is a hole inside the AB contour, it is possible that there are multiple metastable states that can support the total current. These states differ by the number of times the phase winds along paths around the AB contour. The winding number n_v changes whenever a vortex (or an antivortex) passes across one of the wires.

In the present theory, we include two kinds of processes that lead to the generation of a voltage difference between the leads; see Fig. 8. In the first kind of process [Fig. 8(a)], two phase slips occur simultaneously: a vortex passes across the top wire and, concurrently, an antivortex passes across the bottom wire (in the opposite direction), so that the winding number remains unchanged. In the second kind of process [Fig. 8(b)], the phase slips occur sequentially: a vortex (or antivortex) enters the AB contour by passing across the top (or bottom) wire, stays inside the contour for some time interval, and then leaves the AB contour through the bottom (or top) wire.[9]

Our goal is to extend LAMH theory to take into account the influence of the wires on each other. In Appendix C, we review some necessary ingredients associated with the LAMH theory of a single wire. As the wires used in the experiments are relatively short (i.e., 10 to 20 zero-temperature coherence lengths in length), we also take care to correctly treat the wires as being of finite length.

Recall that we are considering experiments performed at a fixed total current, and accordingly, in all configurations of the order parameter this current must be shared between the top and bottom wires. We shall refer to this sharing,

$$I = I_1 + I_2, \tag{32}$$

as the *total current constraint*. Let us begin by considering a phase-slip event in a device with an isolated wire. While the order parameter in that wire pinches down, the end-to-end phase accumulation must adjust to maintain the prescribed value of the current through the wire. Now consider the two-wire device, and consider a phase slip event in one of the wires. As in the single-wire case, the phase accumulation will adjust, but in so doing it will alter the current flowing through the other wire. Thus, in the saddle-point configuration of the two-wire system, the current splitting will differ

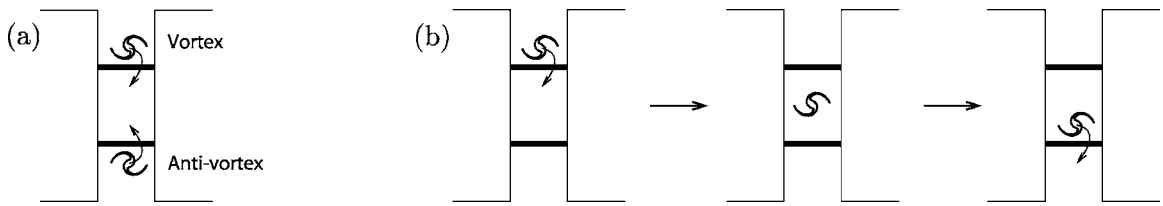

FIG. 8. Thermally activated phase slip processes under consideration. (a) Parallel phase slips. (b) Sequential phase slips.

from that in the locally stable initial (and final) state.

Taking into account the two kinds of phase-slip processes, and imposing the appropriate constraints (i.e., the total current constraint and the phase constraint), we construct the possible metastable and saddle-point configurations of the order parameter in the two-wire system. Finally, we compute the relevant rates of thermally activated transitions between these metastable states, construct a Markov chain,[18] and determine the steady-state populations of these states. Thus, we are able to evaluate the time average of the voltage generated between the leads at fixed current due to these various dissipative fluctuations. We mention that we have not allowed for wires of distinct length or constitution (so that the Ginzburg-Landau parameters describing them are taken to be identical). This is done solely to simplify the analysis; extensions to more general cases would be straightforward but tedious.

1. Parallel pair of nanowires

The total Gibbs free energy for the two-wire system is given by

$$G(I) = F_1(\theta_1) + F_2(\theta_2) - 4\mathcal{E}\Theta(J_1 + J_2). \tag{33}$$

Here, we have followed MH by rewriting the current-phase term in terms of dimensionless currents in wires $i=1,2$, i.e., J_i defined via $I_i = 8\pi c J_i \mathcal{E}/\Phi_0$. Moreover, $\mathcal{E} \equiv H_c^2 \xi \sigma / 8\pi$ is the condensate energy density per unit length of wire, and $F_i(\theta_i)$ is the Helmholtz free energy for a single wire along which there is a total phase accumulation of θ_i. The precise form of $F_i(\theta_i)$ depends on whether the wire is in a metastable or saddle-point state.

We are concerned with making stationary the total Gibbs free energy at specified total current I, subject to the phase constraint, Eq. (2). This can be accomplished by making stationary the Helmholtz free energy on each wire, subject to both the total current constraint and the phase constraint, but allowing θ_1 and θ_2 to vary so as to satisfy these constraints—in effect, adopting the total current I as the independent variable. The stationary points of the Helmholtz free energy for a single wire are reviewed in Appendix C as implicit functions of θ_i, i.e., the end-to-end phase accumulation along the wire. The explicit variable used there is J_i, which is related to θ_i via Eq. (C21).

2. Analytical treatment in the limit of long nanowires

In the long-wire limit, we can compute the resistance analytically by making use of the single-wire free energy and end-to-end phase accumulation derived by Langer and Ambegaokar[14] (and extended by McCumber[17] for the case of the constant-current ensemble). Throughout the present subsection, we shall be making an expansion in powers of $1/b$, where b is the length of the wire measured in units of the coherence length, keeping terms only to first order in $1/b$. Thus, one arrives at formulas for the end-to-end phase accumulations and Helmholtz free energies for single-wire metastable (m) and saddle-point (sp) states,[17]

$$\theta_m(\kappa) = \kappa b, \tag{34a}$$

$$\theta_{\rm sp}(\kappa) = \kappa b + 2\tan^{-1}\left(\frac{1-3\kappa^2}{2\kappa^2}\right)^{1/2}, \tag{34b}$$

$$F_m(\kappa) = -\mathcal{E}[b(1-\kappa^2)^2], \tag{34c}$$

$$F_{\rm sp}(\kappa) = -\mathcal{E}\left(b(1-\kappa^2)^2 - \frac{8\sqrt{2}}{3}\sqrt{1-3\kappa^2}\right), \tag{34d}$$

where κ is defined via $J_i = \kappa_i(1-\kappa_i^2)$. In the small-current limit, one can make the further simplification that $J_i \approx \kappa_i$; henceforth we shall keep terms only up to first order in κ. To this order, the phase difference along a wire in a saddle-point state becomes

$$\theta_{\rm sp} = \kappa b + \pi - 2\sqrt{2}\kappa. \tag{35}$$

Next, we make use of these single-wire LAMH results to find the metastable and saddle-point states of the two-wire system, and use them to compute the corresponding barrier heights and, hence, transition rates. At low temperatures, it is reasonable to expect that only the lowest few metastable states will be appreciably occupied. These metastable states, as well as the saddle-point states between them, correspond to pairs, κ_1 and κ_2, one for each wire, that satisfy the total current constraint as well as the phase constraint,

$$\kappa_1 + \kappa_2 = J, \tag{36}$$

$$\theta_1(\kappa_1) - \theta_2(\kappa_2) = 2\pi n_v + 2\delta, \tag{37}$$

where we need to substitute the appropriate $\theta_{m/\rm sp}(\kappa_i)$ from Eqs. (34a) and (35) for $\theta_i(\kappa_i)$.

In the absence of a magnetic field (i.e., $\delta=0$), the lowest-energy state is the one with no circulating current, and the current split evenly between the two wires. This corresponds to the solution of Eqs. (36) and (37) with $n=0$, together with the substitution (34a) for $\theta_i(\kappa_i)$ for both wires (i.e., $\theta_1 = \kappa_1 b$ and $\theta_2 = \kappa_2 b$). Thus we arrive at the solution

$$\kappa_1 = J/2, \quad \theta_1 = bJ/2, \tag{38a}$$

$$\kappa_2 = J/2, \quad \theta_2 = bJ/2. \tag{38b}$$

If we ignore the lowest (excited) metastable states, then only a parallel phase-slip process is allowed. The saddle point for a parallel phase slip corresponds to a solution of Eqs. (36) and (37) with $n=0$ and the substitution (35) for $\theta_i(\kappa_i)$ for both wires,

$$\kappa_1 = J/2, \quad \theta_1 = bJ/2 + \pi - 2\sqrt{2}J/2, \tag{39a}$$

$$\kappa_2 = J/2, \quad \theta_2 = bJ/2 + \pi - 2\sqrt{2}J/2. \tag{39b}$$

The change in the phase difference across the center of the trench, $\Delta\Theta \equiv (\Theta_{\rm sp} - \Theta_m)$, is $\pi - 2\sqrt{2}\kappa$ for a forward phase slip and $-\pi - 2\sqrt{2}\kappa$ for a reverse phase slip. The Gibbs free-energy barrier for the two kinds of phase slips, computed by subtracting the Gibbs free energy for the ground state from that of the saddle-point state, is

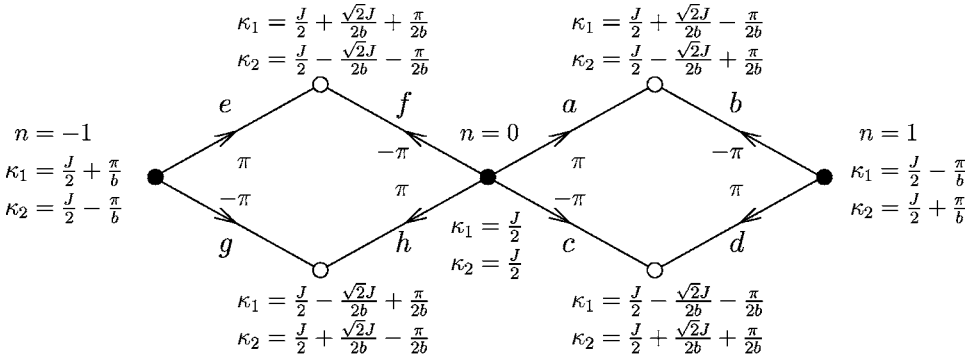

edge	$\Delta\Theta$	$\Delta F/\mathcal{E}$	$\Delta G/\mathcal{E}$	phase
a	$-\frac{\sqrt{2}J}{2} + \frac{\pi}{2}$	$\frac{8\sqrt{2}}{3} + \frac{\pi^2}{b}$	$\frac{8\sqrt{2}}{3} + \frac{\pi^2}{b} - \frac{4\pi J}{2}$	π
b	$-\frac{\sqrt{2}J}{2} - \frac{\pi}{2}$	$\frac{8\sqrt{2}}{3}$	$\frac{8\sqrt{2}}{3} + \frac{4\pi J}{2}$	$-\pi$
c	$-\frac{\sqrt{2}J}{2} - \frac{\pi}{2}$	$\frac{8\sqrt{2}}{3} + \frac{\pi^2}{b}$	$\frac{8\sqrt{2}}{3} + \frac{\pi^2}{b} + \frac{4\pi J}{2}$	$-\pi$
d	$-\frac{\sqrt{2}J}{2} + \frac{\pi}{2}$	$\frac{8\sqrt{2}}{3}$	$\frac{8\sqrt{2}}{3} - \frac{4\pi J}{2}$	π
e	$-\frac{\sqrt{2}J}{2} + \frac{\pi}{2}$	$\frac{8\sqrt{2}}{3}$	$\frac{8\sqrt{2}}{3} - \frac{4\pi J}{2}$	π
f	$-\frac{\sqrt{2}J}{2} - \frac{\pi}{2}$	$\frac{8\sqrt{2}}{3} + \frac{\pi^2}{b}$	$\frac{8\sqrt{2}}{3} + \frac{\pi^2}{b} + \frac{4\pi J}{2}$	$-\pi$
g	$-\frac{\sqrt{2}J}{2} - \frac{\pi}{2}$	$\frac{8\sqrt{2}}{3}$	$\frac{8\sqrt{2}}{3} + \frac{4\pi J}{2}$	$-\pi$
h	$-\frac{\sqrt{2}J}{2} + \frac{\pi}{2}$	$\frac{8\sqrt{2}}{3} + \frac{\pi^2}{b}$	$\frac{8\sqrt{2}}{3} + \frac{\pi^2}{b} - \frac{4\pi J}{2}$	π

FIG. 9. Diagram representing the ground state (central filled circle), the two lowest-energy metastable states (left and right filled circles), and the saddle-point states connecting them (open circles) for the case of magnetoresistance minimum (i.e., $\delta = 0, \pi, \ldots$). The saddle-point states at the top of the graph correspond to phase slips in the top wire (i.e., wire 1); those at the bottom correspond to the bottom wire (i.e., wire 2). (Saddle-point states for parallel phase slips are not shown.) For each state κ_1 and κ_2 are listed. For each barrier (represented by an edge and labeled by a through h), the table at the right lists the gain in phase across the trench, the gain in Helmholtz free energy, the barrier height (i.e., the gain in Gibbs free energy), and the amount of phase that would effectively be generated at the end of the phase slip event (i.e., upon completion of a closed loop, the amount of phase generated is the sum of the effective phases).

$$\Delta G = \mathcal{E}\left(\frac{16\sqrt{2}}{3} \pm 4J\pi\right). \tag{40}$$

The former free energy is obtained by substituting Eq. (34c) into Eq. (33) for both wires; the latter one is obtained by substituting Eq. (34d) into Eq. (33) for both wires. We note that the Gibbs free-energy barrier heights for parallel phase slips (in both the forward and reverse directions) are just double those of the LAMH result for a single wire. From the barrier heights, we can work out the generated voltage by appealing to the Josephson relation, $V=(\hbar/2e)\dot{\Theta}$, and to the fact that each phase slip corresponds to the addition (or subtraction) of 2π to the phase. Hence, we arrive at the current-voltage relation associated with parallel phase slips at $\delta=0$,

$$V_{\delta=0,\mathrm{par}} = \frac{\hbar}{e}\Omega e^{-\beta\mathcal{E}(16\sqrt{2}/3)}\sinh(I/I_0), \tag{41}$$

where the prefactor Ω may be computed using time-dependent Ginzburg-Landau theory or extracted from experiment, and $I_0=4e/\beta h$.

If we take into account the two lowest excited states, which we ignored earlier, then voltage can also be generated via sequential phase slips (in addition to the parallel ones, treated above). To tackle this case, we construct a diagram in which the vertices represent the metastable and saddle-point solutions of Eqs. (36) and (37), and the edges represent the corresponding free-energy barriers; see Fig. 9. Pairs of metastable-state vertices are connected via two saddle-point-state vertices, corresponding to a phase slip on either the top or the bottom wire. To go from one metastable state to another, the system must follow the edge out of the starting metastable state leading to the desired saddle-point state. We assume that, once the saddle-point state is reached, the top of the barrier has been passed and the order parameter relaxes to the target metastable state. (To make the graph more legible, we have omitted drawing the edge that corresponds to this relaxation process.) To find the Gibbs free-energy difference between a metastable state and a saddle-point state, we need to know the phase difference across the center of the trench. To resolve the ambiguity of 2π in the definition of Θ, the phase difference can be found by following the wire with no phase slip. To further improve the legibility of Fig. 9, the free-energy barriers are listed in a separate table to the right. Note that a phase slip on just one of the wires, being only half of the complete process, can be regarded as a gain in phase of $\pm\pi$ for the purposes of calculating voltage, as indicated in both the graph and the table.

Once the table of barrier heights has been computed, we can construct a Markov chain on a directed graph, where the metastable states are the vertices—in effect, an explicit version of our diagram. In general, each pair of neighboring metastable states, s_n and s_{n+1}, is connected by four directed edges,

$$s_n \xrightarrow[\text{top}]{} s_{n+1}, \quad s_n \xrightarrow[\text{bottom}]{} s_{n+1}, \tag{42a}$$

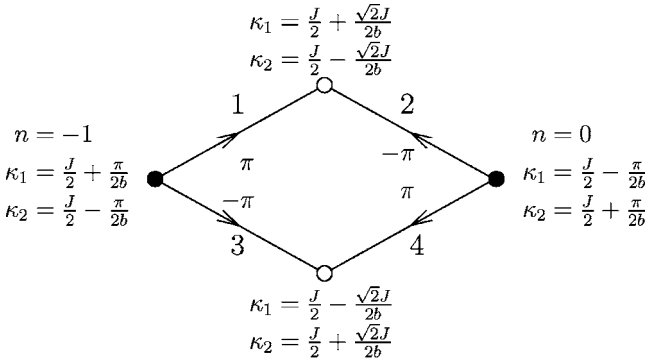

edge	$\Delta\Theta$	$\Delta F/\mathcal{E}$	$\Delta G/\mathcal{E}$	phase
1	$-\frac{\sqrt{2}J}{2} + \frac{\pi}{2}$	$\frac{8\sqrt{2}}{3} - \frac{\pi^2}{b}$	$\frac{8\sqrt{2}}{3} - \frac{\pi^2}{b} - \frac{4\pi J}{2}$	π
2	$-\frac{\sqrt{2}J}{2} - \frac{\pi}{2}$	$\frac{8\sqrt{2}}{3} - \frac{\pi^2}{b}$	$\frac{8\sqrt{2}}{3} - \frac{\pi^2}{b} + \frac{4\pi J}{2}$	$-\pi$
3	$-\frac{\sqrt{2}J}{2} - \frac{\pi}{2}$	$\frac{8\sqrt{2}}{3} - \frac{\pi^2}{b}$	$\frac{8\sqrt{2}}{3} - \frac{\pi^2}{b} + \frac{4\pi J}{2}$	$-\pi$
4	$-\frac{\sqrt{2}J}{2} + \frac{\pi}{2}$	$\frac{8\sqrt{2}}{3} - \frac{\pi^2}{b}$	$\frac{8\sqrt{2}}{3} - \frac{\pi^2}{b} - \frac{4\pi J}{2}$	π

FIG. 10. Diagram and corresponding table for the case of magnetoresistance maxima (i.e., $\delta=\pi/2,3\pi/2,\ldots$). See the caption to Fig. 9 for explanation of the diagram.

$$s_n \xleftarrow[\text{top}]{} s_{n+1}, \quad s_n \xleftarrow[\text{bottom}]{} s_{n+1}, \tag{42b}$$

where the probability to pass along a particular edge is given by $P(\cdot)=\exp-\beta\Delta G_{(\cdot)}$, in which $\Delta G_{(\cdot)}$ may be read off from the table in Fig. 9.

We denote the occupation probability of the nth metastable state by o_n, where n corresponds to the n in the phase constraint (2). o_n may be computed in the standard way, by diagonalizing the matrix representing the Markov chain.[18] Each move in the Markov chain can be associated with a gain in phase across the device of $\pm\pi$, as specified in Fig. 9. Thus, we may compute the rate of phase gain, and hence the voltage

$$V = \frac{\Omega\hbar}{4e}\sum_{\langle nm\rangle}\frac{o_n}{g_{n,m}}[P(s_n \xrightarrow[\text{top}]{} s_m) - P(s_n \xrightarrow[\text{bot}]{} s_m)], \tag{43}$$

where the rate prefactor Ω is to be determined, $\langle nm\rangle$ indicates that the sum runs over neighboring states only, and $g_{n,m}$ keeps track of the sign of the phase gain for reverse phase slips,

$$g_{n,m} = \begin{cases} 1 & \text{if } m > n, \\ -1 & \text{if } m < n. \end{cases} \tag{44}$$

For the case $\delta=0$, and keeping the bottom three states only, the voltage generated via sequential phase slips turns out to be

$$V_{\delta=0,\text{seq}} = \frac{2\hbar}{e}\Omega e^{-\beta\mathcal{E}[(8\sqrt{2}/3)+(\pi^2/b)]}\sinh(I/2I_0). \tag{45}$$

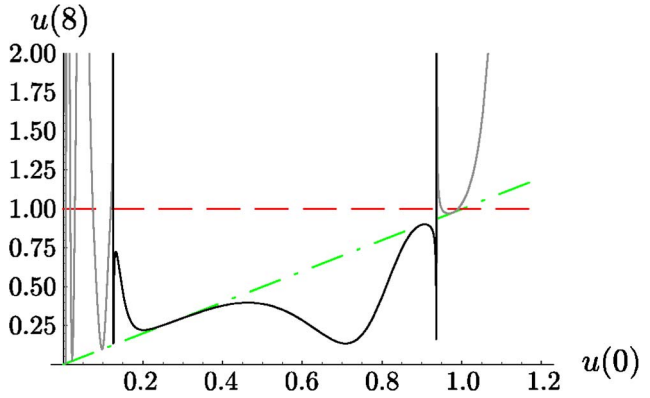

FIG. 11. (Color online) Squared amplitude $u(b/2)$ of the order parameter at the end of a wire, as a function of its value $u_0=u(0)$ at the midpoint of the wire, computed using the JacobiSN function [see Eq. (C20b)], for the case $b=16$, $J=0.235$. The black line corresponds to trajectories that do not go through a pole; the gray line corresponds to trajectories that do pass through at least one pole. The intersection of the dashed and black lines represents those trajectories that satisfy the boundary condition $u(\pm b/2)=1$. [The intersection of the dashed-dotted and black lines represents trajectories that start and stop at the same point, i.e., $u(b/2)=u_0$].

Having dealt with the case of $\delta=0$ (and hence obtained the value of the resistance at magnetic fields corresponding to resistance minima), we now turn to the case of $\delta=\pi/2$, i.e., resistance maxima.

In this half-flux quantum situation, there are two degenerate lowest-energy states, with opposite circulating currents. These states are connected by saddle-point states in which a phase slip is occurring on either the top or bottom wire. The diagram of the degenerate ground states and the saddle-point states connecting them is shown in Fig. 10. By comparing the diagram with the associated table, it is easy to see that the free-energy barriers are biased by the current, making clockwise traversals of Fig. 10 more probable than counterclockwise traversals. As there are only two metastable states being considered, and as they are degenerate, it is unnecessary to go through the Markov chain calculation; clearly, the two states each have a population of $\frac{1}{2}$. The voltage being generated by the sequential phase slip is then given by

$$V_{\delta=\pi/2,\text{seq}} = \frac{\hbar}{2e}\Omega e^{-\beta\mathcal{E}[(8\sqrt{2}/3)-(\pi^2/b)]}\sinh(I/2I_0). \tag{46}$$

$V_{\delta=\pi/2,\text{seq}}$ is larger than the sum of $V_{\delta=0,\text{seq}}$ and $V_{\delta=0,\text{par}}$, so, as expected, the resistance is highest at magnetic fields corresponding to $\delta=\pi/2$. For very long wires, the perturbation of one wire when a phase slip occurs in the other is very small, and therefore we expect that the dependence of resistance on magnetic field will decrease with wire length. Indeed, for very long wires, the difference in barrier heights to sequential phase slips between the $\delta=0$ and $\delta=\pi/2$ cases disappears [i.e., Eq. (45) and (46) agree when $b\gg 1$].

3. Numerical treatment for intermediate-length nanowires

Instead of using the long-wire approximation, Eqs. (34a)–(34d), we can use the exact functions for the end-to-

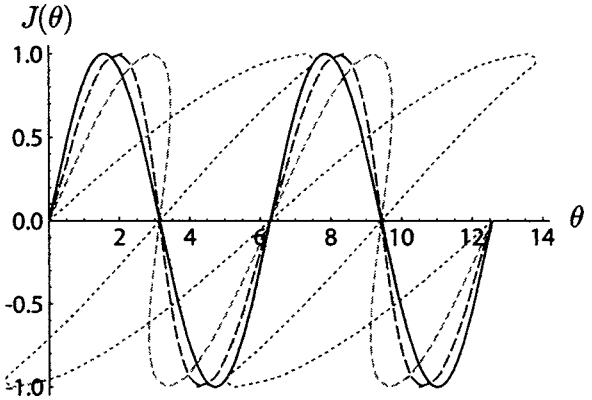

FIG. 12. Current (in units of the critical current) vs end-to-end phase accumulation for superconducting wires of various lengths: 0ξ (solid line), 1.88ξ, 5.96ξ, 14.4ξ (dotted line). The transition from LAMH to Josephson junction behavior is evident from the loss of multivaluedness of the current, as the wire length is reduced.

end phase accumulation along a wire $\theta(J(\kappa))$ and the Helmholtz free energy $F_{m/\mathrm{sp}}(J(\kappa))$. By dropping the long-wire approximation, as the temperature approaches T_c and the coherence length decreases, the picture correctly passes to the Josephson limit. In this approach, the total current and the phase constraints must be solved numerically, as $\theta(J(\kappa))$ is a relatively complicated function. Figure 12 provides an illustration of how, for a single wire, the function $J(\theta)$ depends on its length. We shall, however, continue to use the barrier-crossing approximation. Because the barriers get shallower near T_c, our results will become unreliable (and, indeed, incorrect) there.

The form of the order parameter that satisfies the Ginzburg-Landau equation inside the wire is expressed in Eqs. (C20b) and (C6). Therefore, to construct the functions $\theta(J)$ and $F_{m/\mathrm{sp}}(J)$ [i.e., Eqs. (C21) and (C22)], we need to find $u_0(J)$, i.e., the squared amplitude of the order parameter in the middle of the wire. Hence, we need to ascertain suitable boundary conditions obeyed by the order parameter at the ends of the wire, and use the relation between the squared amplitude of the order parameter in the middle of the wire and at the edges (see Fig. 11).[23] For thin wires, a reasonable hypothesis is that the amplitude of the order parameter at the ends of the wire matches the amplitude in the leads,

$$f(z = \pm b/2)^2 = \frac{H_{c\mathrm{film}}^2(T)\xi_{\mathrm{film}}^2(T)}{H_{c\mathrm{wire}}^2(T)\xi_{\mathrm{wire}}^2(T)}. \tag{47}$$

For wires made out of superconducting material the same as (or weaker than) the leads, this ratio is always larger than unity.[23]

Once we have computed the functions $\theta(J)$ and $F_{m/\mathrm{sp}}(J)$ for both saddle-point and metastable states on a single wire, we can use the phase and total current constraints to build the saddle-point and metastable states for the two-wire device. We proceed as before, by constructing a Markov chain for the state of the device, except that now we include in the graph all metastable states of the device. By diagonalizing the Markov chain, we find the populations of the various metastable states and, hence, the rate of gain of Θ.

V. CONNECTIONS WITH EXPERIMENT

In this section, a connection is made between our calculations and our experiments.[5] First, the predicted period of the magnetoresistance oscillations is compared to the experimentally obtained one. Then, the experimentally obtained resistance versus temperature curves are fitted using our extension of the IZAH Josephson junction model (for shorter wires) and our extension of the LAMH wire model (for longer wires).

A. Device fabrication

Four different devices were successfully fabricated and measured. The devices were fabricated by suspending DNA molecules across a trench and then sputter-coating them with the superconducting alloy of MoGe. The leads were formed in the same sputter-coating step, ensuring seamless contact between leads and the wires. Next, the leads were truncated lithographically to the desired width. In the case of device 930-1, after being measured once, its leads were further narrowed using focused ion beam milling, and the device was remeasured. For further details of the experimental procedure, see Ref. 5.

B. Comparison between theory and experiment

1. Oscillation period

The magnetoresistance periods obtained for four different samples are summarized in Table I. The corresponding theoretical periods were calculated using Eq. (6), based on the geometry of the samples, which was obtained via scanning electron microscopy. To test the theoretical model, the leads of one sample, sample 930-1, were narrowed using a focused ion beam mill, and the magnetoresistance of the sample was remeasured. The theoretically predicted periods all coincide quite well with the measured values, except for sample 219-4, which was found to have a "+" shaped notch in one of the leads (which was not accounted for in calculating the period). The notch effectively makes that lead significantly narrower, thus increasing the magnetoresistance period, and this qualitatively accounts for the discrepancy.

For all samples, when the leads are driven into the vortex state, the magnetoresistance period becomes much longer, approaching the Aharonov-Bohm value for high fields. This is consistent with the theoretical prediction that the period is then given by Eq. (6), but with l replaced by the field-dependent intervortex spacing r.

2. Oscillation amplitude

We have made qualitative and quantitative estimates of the resistance of two-bridge devices in several limiting cases. For devices containing extremely short wires $[b \approx \xi(T)]$, such as sample 219-4, the superconducting wires cannot support multiple metastable states, and thus they operate essentially in the Josephson junction limit, but with the junction

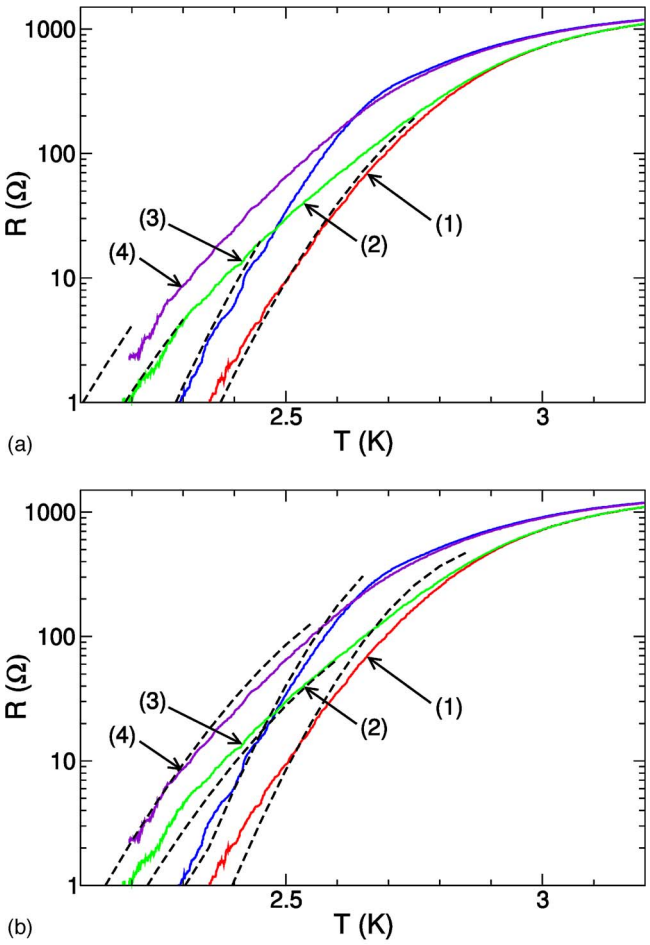

(LHS) $R_1 = 2882.9\,\Omega$, $R_2 = 2941.7\,\Omega$, $\xi_{01} = 17.3\,\mathrm{nA}$,
$\xi_{02} = 8.7\,\mathrm{nA}$, $T_{c1} = 3.147\,\mathrm{K}$, $T_{c2} = 3.716\,\mathrm{K}$.

(RHS) $R_1 = 2912\,\Omega$, $R_2 = 2912\,\Omega$, $\xi_{01} = 10\,\mathrm{nA}$,
$\xi_{02} = 9\,\mathrm{nA}$, $T_{c1} = 3\,\mathrm{K}$, $T_{c2} = 3.65\,\mathrm{K}$.

FIG. 13. (Color online) Sample 930-1: Resistance vs temperature curves. Experimental data (full lines) and theoretical fits using the LAMH-type model in the intermediate regime (dashed lines). Theoretical curves terminate when the short-wire regime is reached, i.e., $5\xi(T) \sim b$. (1) Zero magnetic field and low total current. (2) Magnetic field set to maximize the magnetoresistance and low total current. (3) Zero magnetic field and 80 nA total current. (4) Magnetic field set to maximize the resistance and 80 nA total current. The fit on the left was optimized numerically, and the one on the right was obtained by hand, showing that a more realistic value of ξ_{01} remains reasonably consistent.

critical current being a function of temperature given by LAMH theory as $I_c(T) = I_c(0)(1 - T/T_c)^{3/2}$. A summary of fits to the data for this sample, using the Josephson junction limit, is shown in Fig. 7. On the other hand, for longer wires it is essential to take into account the multiple metastable states, as is the case for sample 930-1, which has wires of intermediate length. A summary of numerical fits for this sample is shown in Fig. 13. In all cases, only the two low total-current magnetoresistance curves were fitted. By using the extracted fit parameters, the high total-current magnetoresistance curves were calculated, with their fit to the data serving as a self-consistency check. As can be seen from the fits, our model is consistent with the data over a wide range of temperatures and resistances. We remark, however, that the coherence length required to fit the data is somewhat larger than expected for MoGe.

VI. CONCLUDING REMARKS

The behavior of mesoscale NQUIDs composed of two superconducing leads connected by a pair of superconducting nanowires has been investigated. Magnetoresistance measurements[5] have revealed strong oscillations in the resistance as a function of magnetic field, and these were found to have anomalously short periods. The period has been shown to originate in the gradients in the phase of the superconducting order parameter associated with screening currents generated by the applied magnetic field. The periods for five distinct devices were calculated, based on their geometry, and were found to fit very well with the experimental results.

The amplitude of the magnetoresistance has been estimated via extensions, to the setting of parallel superconducting wires, of the IZAH theory of intrinsic resistive fluctuations in a current-biased Josephson junction for the case of short wires and the LAMH theory of intrinsic resistive fluctuations in superconducting wires for pairs of long wires. In both cases, to make the extensions, it was necessary to take into account the interwire coupling mediated through the leads. For sufficiently long wires, it was found that multiple metastable states, corresponding to different winding numbers of the phase of the order parameter around the AB contour, can exist and need to be considered. Accurate fits have been made to the resistance versus temperature data at various magnetic fields and for several devices by suitably tuning the critical temperatures, zero-temperature coherence lengths, and normal-state resistances of the nanowires.

As these device are sensitive to the spatial variations in the phase of the order parameter in the leads, they may have applications as superconducting phase gradiometers. Such applications may include the sensing of the presence in the leads of vortices or of supercurrents flowing perpendicular to lead edges.

ACKNOWLEDGMENTS

This work was supported by the U.S. Department of Energy, Division of Materials Sciences under Award No. DEFG02-91ER45439, through the Frederick Seitz Materials Research Laboratory at the University of Illinois at Urbana-Champaign. AB and DH would like to also acknowledge support from the Center for Microanalysis of Material DOE Grant No. DEFG02-96ER45439, NSF CAREER Grant No. DMR 01-34770, and the A.P. Sloan Foundation.

APPENDIX A: MULTIWIRE DEVICES

In this appendix, we give an example of how to extend the theory presented in this paper to the case of devices comprising more than two wires. In our example, we consider an array of n identical short wires (i.e., wires in the Josephson

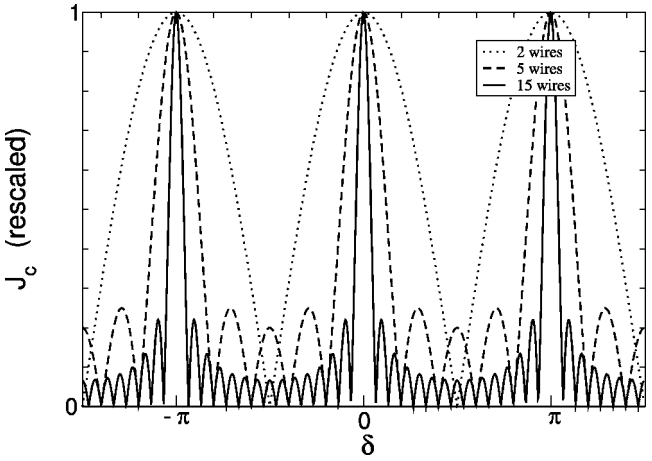

FIG. 14. Effective single junction critical current for a multijunction array, as a function of δ. The critical current has been rescaled so that $J_c(\delta=0)=1$. Note the similarity with a multislit interference pattern.

junction limit) spaced at regular intervals. We continue to work at a fixed total current and to ignore charging effects. The end-to-end phase accumulations along the wires are related to each other as

$$\theta_2 = \theta_1 + 2\delta,$$

$$\theta_3 = \theta_1 + 4\delta,$$

$$\vdots$$

$$\theta_n = \theta_1 + 2(n-1)\delta, \tag{A1}$$

i.e., $\theta_n - \theta_1 = 2(n-1)\delta$ (for $n=2,\ldots,N$), where δ is the phase accumulation in one of the leads between each pair of adjacent wires. The Gibbs free energy of the multiwire subsystem is given by

$$G(I,\theta_1) = -\frac{h}{2e}\left(I_c \sum_{m=1}^{n} \cos[\theta_1 + 2(m-1)\delta] + I\theta_1\right), \tag{A2}$$

where I is the total current and we are assuming that the wires have identical critical currents. As for the two-junction case, this junction array is equivalent to a single effective junction. Figure 14 shows the critical current of this effective junction as a function of δ for devices comprising 2, 5, and 15 wires. The magnetoresistance of such a device then follows from IZAH theory, i.e., Eq. (31).

APPENDIX B: PHYSICAL SCALES

It is convenient to express the results of the long-wire model, Eqs. (41), (45), and (46), in terms of macroscopic physical parameters. Following Tinkham and Lau,[19] we express the condensation energy scale per coherence length of wire as

$$\mathcal{E} = 0.22 k_B T_c (1-t)^{3/2} \frac{R_q}{R_N} \frac{b}{\xi(T=0)}, \tag{B1}$$

where $t \equiv T/T_c$, R_N is the normal-state resistance of the device, and $R_q \equiv h/4e^2 \approx 6.5\ \mathrm{k}\Omega$ is the quantum of resistance. The LAMH prefactor for sequential phase slips then becomes

$$\Omega = \frac{b\sqrt{1-t}}{\xi(T=0)} \left(\frac{8\sqrt{2}\mathcal{E}}{3k_B T_c}\right)^{1/2} \frac{8k_B(T_c - T)}{\pi\hbar}, \tag{B2}$$

and for parallel phase slips becomes

$$\Omega = \left(\frac{b\sqrt{1-t}}{\xi(T=0)}\right)^2 \left(\frac{16\sqrt{2}\mathcal{E}}{3k_B T_c}\right)^{1/2} \frac{8k_B(T_c - T)}{\pi\hbar}. \tag{B3}$$

The remaining parameters in the model are R_N, T_c, and $\xi(T=0)$. The normal-state resistance and the critical temperature may be obtained from the R versus T curve. The coherence length may be obtained by comparing $\mathcal{E}$ obtained from the critical current at low temperature, via

$$I_c = \frac{2}{3\sqrt{3}} \frac{16\pi\mathcal{E}}{\Phi_0}, \tag{B4}$$

with $\mathcal{E}$ obtained via Eq. (B1).

In experiment, it is expected that the two wires are not identical. The long-wire model can be easily extended to this case. The number of parameters to be fitted would then expand to include the normal-state resistance for each wire (only one of which is free, as the pair are constrained by the normal-state resistance of the entire device, which can be extracted from the R versus T curve), a zero-temperature coherence length for each wire, and a critical temperature for each wire.

APPENDIX C: LAMH THEORY FOR A SINGLE BRIDGE

In this appendix, we reproduce useful formulas from LA,[14] and rewrite them in a way that is convenient for further calculations, especially for numerical implementation. As in the case of single-wire LAMH theory, one starts with the Ginzburg-Landau free energy

$$F = \int_{-b/2}^{b/2} \alpha|\psi|^2 + \frac{\beta}{2}|\psi|^4 + \frac{\hbar^2}{2m}|\nabla\psi|^2 dz. \tag{C1}$$

The relationships between the parameters of the Ginzburg-Landau free energy (α and β), coherence length ξ, the condensation energy per unit coherence length $\mathcal{E}$, the critical field H_c, and the cross-sectional area of the wire σ are given by $\alpha^2/\beta = H_c^2\sigma/8\pi = \mathcal{E}/\xi$ and $\xi^2 = \hbar^2/2m|\alpha|$. Following McCumber,[17] it is convenient to work in terms of the dimensionless units obtained using the transformations $|\psi|^2 \to (\alpha/\beta)|\psi|^2$, $z \to \sqrt{(2m|\alpha|/\hbar^2)}z$, and $b \to b/\xi = \sqrt{(2m|\alpha|/\hbar^2)}b$. In terms of these units, the free energy becomes

$$F = 2\mathcal{E}\int_{-b/2}^{b/2} \left(\frac{1}{2}(1-|\psi|^2)^2 + |\nabla\psi|^2\right) dz. \tag{C2}$$

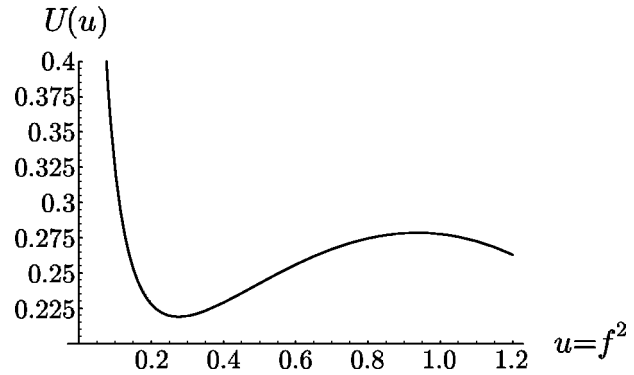

FIG. 15. "Mechanical potential" $U[u=f^2]$ at an intermediate value of the dimensionless current, plotted as a function of amplitude squared to make comparison with Fig. 11 more convenient.

The Ginzburg-Landau equation is obtained by varying the free energy,

$$\delta F = 0 \Rightarrow -\psi + |\psi|^2\psi - \nabla^2\psi = 0. \tag{C3}$$

By writing $\psi = fe^{i\phi}$ and taking the real and imaginary parts of the Ginzburg-Landau equation, one obtains

$$-f + f^3 + (\phi')^2 f = f'', \tag{C4}$$

$$2\phi' f' + \phi'' f = 0. \tag{C5}$$

From Eq. (C5), one finds the current conservation law,

$$f^2\phi' = J, \tag{C6}$$

where J is identified with the dimensionless current $(1/2i)(\psi^*\nabla\psi - \psi\nabla\psi^*)$. The physical current (in stat-amps) is given by $I = JcH_c^2\sigma\xi/\Phi_0$. Expressing ϕ' in terms of J, Eq. (C4) becomes

$$f'' = -f + f^3 + \frac{J^2}{f^3} = -\frac{d}{df}U(f), \tag{C7}$$

where the effective potential $U(f)$ is given by

$$U(f) = \frac{J^2}{2f^2} + \frac{f^2}{2} - \frac{f^4}{4}. \tag{C8}$$

Following LA, Eq. (C8) can usefully be regarded as the equation of motion for a particle with position $f(z)$, where z plays the role of time, moving in the potential $U(f)$.[14] Before proceeding to find the solution of this equation, we pause to consider the type of trajectories that are possible. Later, it will be demonstrated that at the edge of the wire $f(\pm b) \geqslant 1$, so the particle starts to the right of the hump; see Fig. 15. If the total energy of the particle is less than the height of the hump, the particle will be reflected by the hump. If, however, the particle starts with more energy than the height of the hump, it will pass over the hump and be reflected by the $J^2/2f^2$ dominated part of $U(f)$.

The equation of motion can be solved via the first integral (i.e., multiplying both sides by f and integrating with respect to f),

$$E = \frac{(f')^2}{2} + U(f) \Rightarrow f' = \sqrt{2[E - U(f)]}, \tag{C9}$$

where E is a constant of integration (i.e., the energy of the particle in the mechanical analogy), which gives

$$z = \int_{f_0}^{f} \frac{df}{\sqrt{2[E - U(f)]}} = \int_{f_0}^{f} \frac{fdf}{\sqrt{2f^2E - J^2 - f^4 + f^6/2}}. \tag{C10}$$

It is convenient to apply "initial" conditions at the middle of the wire, where $f(z=0)=f_0$, and to integrate toward the edges. We require that the particle come back to its starting point after a "time" b, i.e., at the edges of the wire the amplitude of the order parameter must match the boundary condition. Therefore, the middle of the wire must be the turning point for the particle, i.e., at $z=0$ we have $E=U(f_0)$.

What follows next is a series of manipulations via which one can express solution for $f(z)$ in terms of special functions.

Step 1: substitution: $f^2 \to u$,

$$z = \frac{1}{2}\int_{u_0}^{u} \frac{du}{\sqrt{2Eu - J^2 - u^2 + u^3/2}}. \tag{C11}$$

Step 2: substitution: $u \to u_0 + \epsilon$,

$$2z = \int_0^{u-u_0} \frac{d\epsilon}{\left\{\epsilon\left[\underbrace{\left(\frac{J^2}{u_0} - u_0 + u_0^2\right)}_{\alpha} + \underbrace{\left(\frac{3}{2}u_0 - 1\right)}_{\beta}\epsilon + \epsilon^2/2\right]\right\}^{1/2}}, \tag{C12}$$

$$2z = \int_0^{u-u_0} \frac{d\epsilon}{\left\{\epsilon\left[\underbrace{\left(\frac{J^2}{u_0} - u_0 + u_0^2\right)}_{\alpha} + \underbrace{\left(\frac{3}{2}u_0 - 1\right)}_{\beta}\epsilon + \epsilon^2/2\right]\right\}^{1/2}},$$

$$2z = \int_0^{u-u_0} \frac{d\epsilon}{[\epsilon(\epsilon + \beta\epsilon + \epsilon^2/2)]^{1/2}} \tag{C13}$$

$$= \int_0^{u-u_0} \frac{\sqrt{2}d\epsilon}{[\epsilon(\epsilon + \underbrace{\beta + \sqrt{\beta^2 - 2\alpha}}_{-u_1})(\epsilon + \underbrace{\beta - \sqrt{\beta^2 - 2\alpha}}_{-u_2})]^{1/2}} \tag{C14}$$

$$= \int_0^{u-u_0} \frac{\sqrt{2}d\epsilon}{[\epsilon(\epsilon + \beta + \underbrace{\sqrt{\beta^2 - 2\alpha}}_{-u_1})(\epsilon + \beta - \underbrace{\sqrt{\beta^2 - 2\alpha}}_{-u_2})]^{1/2}}$$

$$= \int_0^{u-u_0} \frac{\sqrt{2}d\epsilon}{[\epsilon(\epsilon - u_1)(\epsilon - u_2)]^{1/2}}. \tag{C15}$$

Step 3: substitution: $\epsilon \to u_1 z^2$,

$$2z = \frac{2\sqrt{2}}{\sqrt{u_2}}\int_0^{\sqrt{(u-u_0)/u_1}} \frac{d\omega}{\left[(\omega^2 - 1)\left(\frac{u_1}{u_2}\omega^2 - 1\right)\right]^{1/2}} \tag{C16}$$

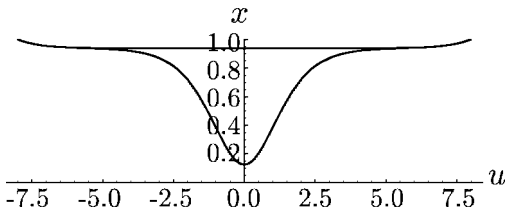

FIG. 16. Squared amplitude u of the order parameter as a function of position along the wire for the two types of solution: metastable and saddle point.

$$= \frac{2\sqrt{2}}{\sqrt{u_2}} \text{EllipticF}\left[\text{ArcSin}\left[\sqrt{\frac{u-u_0}{u_1}} \right], \frac{u_1}{u_2} \right]. \quad \text{(C17)}$$

The following definitions have been used:

$$\alpha[u_0] \equiv J^2/u_0 - u_0 + u_0^2, \quad \beta[u_0] \equiv \frac{3}{2}u_0 - 1, \quad \text{(C18)}$$

$$u_1[\alpha,\beta] \equiv -\beta - \sqrt{\beta^2 - 2\alpha}, \quad u_2[\alpha,\beta] \equiv -\beta + \sqrt{\beta^2 - 2\alpha}. \quad \text{(C19)}$$

By inverting relation (C17), one obtains an explicit equation for the amplitude of the order parameter as a function of position along the wire (see Fig. 16),

$$f^2(z) = u_0 + u_1 \sin^2\left[\text{JacobiAmplitude}\left[z\sqrt{\frac{u_2}{2}}, \frac{u_1}{u_2} \right] \right] \quad \text{(C20a)}$$

$$= u_0 + u_1 \text{JacobiSn}^2\left[z\sqrt{\frac{u_2}{2}}, \frac{u_1}{u_2} \right]. \quad \text{(C20b)}$$

The end-to-end phase difference along the wire may be found by using the current conservation law. Thus one obtains

$$\theta = \int_{-b/2}^{b/2} \frac{J}{f^2(z)} dz = 2J \int_0^{b/2} \frac{dz}{u_0 + u_1 \text{JacobiSn}^2\left[z\sqrt{\frac{u_2}{2}}, \frac{u_1}{u_2} \right]}. \quad \text{(C21)}$$

The Helmholtz free energy can be found by substituting the expressions for $f(z)$ and $\phi'(z)$ into the expression for the free energy. One then obtains

$$F = 4\mathcal{E} \int_0^{b/2} dz \left(\frac{1}{2} - 2f^2 + f^4 + J^2/u_0 + u_0 - u_0^2/2 \right), \quad \text{(C22)}$$

where E was expressed in terms of u_0. Equations (C21) and (C22) provide expressions for θ and F which are true regardless of the length of the wire, and therefore may be used as a starting point for computing the Gibbs free energy of the various metastable states subject to the total current and the phase constraints.

[1] W. A. Little and R. D. Parks, Phys. Rev. Lett. **9**, 9 (1962); Phys. Rev. **133**, A97 (1964).

[2] M. Tinkham, *Introduction to Superconductivity* (McGraw-Hill, New York, 1996).

[3] K. K. Likharev, Rev. Mod. Phys. **51**, 101 (1979).

[4] A. Bezryadin and B. Pannetier, J. Low Temp. Phys. **98**, 251 (1995); C. C. Abilio, L. Amico, R. Fazio, and B. Pannetier, *ibid.* **118**, 23 (2000).

[5] D. S. Hopkins, D. Pekker, P. M. Goldbart, and A. Bezryadin, Science **308**, 1762 (2005).

[6] See, e.g., C. A. Brebbia, *Boundary Element Method for Engineers* (Pentech Press, London, 1978).

[7] F. London and H. London, Proc. R. Soc. London, Ser. A **A109**, 71 (1935); see also Ref. 2, pp. 4–6

[8] K. K. Likharev, Sov. Radiophys. **14**, 722 (1973); see also J. R. Clem, Bull. Am. Phys. Soc. **43**, 411 (1972); G. M. Maksimova, Phys. Solid State **40**, 1610 (1998).

[9] Here and elsewhere, we speak of *vortices* and *antivortices* entering or leaving the leads or the loop made by the wires. Of course, outside the superconducting regions there can be no vortices or antivortices. Nevertheless, we use this language to connote the temporary reduction of the amplitude of the superconducting order parameter during a dissipative fluctuation, and its global consequences for the phase of the order parameter.

[10] G. Stan, S. B. Field, and J. M. Martinis, Phys. Rev. Lett. **92**, 097003 (2004).

[11] See, e.g., I. S. Gradshtein and I. M. Ryzhik, *Table of Integrals, Series, and Products* (Academic Press, New York, 1965), p. 1036.

[12] Yu. M. Ivanchenko and L. A. Zil'berman, JETP Lett. **8**, 113 (1968); Yu. M. Ivanchenko and L. A. Zil'berman, JETP **28**, 1272 (1969).

[13] V. Ambegaokar and B. I. Halperin, Phys. Rev. Lett. **22**, 1364 (1969).

[14] J. S. Langer and V. Ambegaokar, Phys. Rev. **164**, 498 (1967).

[15] D. E. McCumber and B. I. Halperin, Phys. Rev. B **1**, 1054 (1970).

[16] W. A. Little, Phys. Rev. **156**, 396 (1967).

[17] D. E. McCumber, Phys. Rev. **172**, 427 (1968).

[18] A Markov chain is a device for computing the properties of stochastic processes where each step depends only on the step preceeding it. See, e.g., J. Zinn-Justin, *Quantum Field Theory and Critical Phenomena*, 3rd ed. (Oxford University Press, New York, 2002), p. 79.

[19] M. Tinkham and C. N. Lau, Appl. Phys. Lett. **80**, 2946 (2002).

[20] Consider the case in which $\boldsymbol{A}$ is a London gauge everywhere (with our choice of gauge, $\boldsymbol{A} = By\boldsymbol{e}_x$, this is the case for an infinitely long strip). By using the requirement that $\nabla \cdot \boldsymbol{A} = 0$, together with Eq. (13b), we see that ϕ satisfies the Laplace equation. We further insist that no current flows out of the

superconductor, i.e., along all surfaces the supercurrent density, Eq. (12), is always parallel to the surface. Together with the requirement that along all surfaces $\boldsymbol{A}$ is parallel to them, this implies the boundary condition that $\boldsymbol{n}\cdot\boldsymbol{\nabla}\phi=0$. Next, it can be shown that this boundary condition implies that ϕ must be a constant function of position in order to satisfy the Laplace equation, and therefore Eq. (12) simplifies to read $\boldsymbol{J}=-(c/8\pi\lambda_{\mathrm{eff}}^2)\boldsymbol{A}$, which is known as the London relation.

[21] This specialization is not necessary, but it is convenient and adequately illustrative.

[22] Recall that the Helmholtz free energy is obtained by minimizing the Ginzburg-Landau free-energy functional with respect to the order-parameter function $\psi(\boldsymbol{r})$, subject to the phase accumulation constraint $\int_{\mathrm{L}}^{\mathrm{R}} d\boldsymbol{r}\cdot\boldsymbol{\nabla}\phi=\theta$.

[23] In finding u_0, there is a minor numerical difficulty. As the amplitude of the order parameter is expressed via the JacobiSn function, and JacobiSn$[z\sqrt{u_2/2},u_1/u_2]$ is a doubly periodic function in the first variable, it is not obvious whether $\pm(b/2)\sqrt{u_2/2}$ lies in the first period, as can be seen from Fig. 11. As the trajectory must be simply periodic, $z\sqrt{u_2/2}$ must intersect either a zero or a pole in the first unit quarter cell of the JacobiSn function. Now, we are only interested in trajectories that escape to $f\to\infty$ [as $f(\pm b/2)$ is assumed to be greater than or equal to unity], so a pole must be intersected. (However, being outside the first period is unphysical, as it means that somewhere along the wire $f=\infty$.) There are exactly two poles in the first unit quarter cell. They are located at $2v_1+v_2$ and v_2, where $v_1\equiv \mathrm{K}(u_1/u_2)$ and $v_2\equiv i\mathrm{K}(1-u_1/u_2)$, in which $\mathrm{K}(\cdot)$ is the complete elliptic integral. So, instead of checking whether $\pm(b/2)\sqrt{u_2/2}$ is outside the unit quarter cell, we can just determine which pole $z\sqrt{u_2/2}$ intersects and then see if $\pm(b/2)\sqrt{u_2/2}$ lies beyond that pole or not.